



Observations of fresh, anticyclonic eddies in the Hudson Strait outflow

David A. Sutherland^{a,*}, Fiammetta Straneo^b, Steven J. Lentz^b, Pierre Saint-Laurent^c

^a School of Oceanography, University of Washington, Box 355351, Seattle, WA 98195-5351, United States

^b Department of Physical Oceanography, Woods Hole Oceanographic Institution, MS #21, Woods Hole, MA 02543, United States

^c Institut des Sciences de la Mer, Université de Québec à Rimouski, 310, allée des Ursulines, Rimouski, QC, Canada G5L 3A1

ARTICLE INFO

Article history:

Received 1 February 2010

Received in revised form 10 September 2010

Accepted 4 December 2010

Available online 16 December 2010

Keywords:

Hudson Strait

Hudson Bay

Labrador Current

Freshwater

ABSTRACT

The waters that flow out through Hudson Strait, a coastal system that connects Hudson Bay with the Labrador Sea, constitute the third largest freshwater contribution to the northern North Atlantic. Recent studies have documented the mean structure and transport of the outflow, as well as highlighting significant variability on synoptic scales (days–week). This study examines the outflow's variability on these synoptic scales through the use of observations collected by a mooring array from 2005 to 2006. We focus on the mechanisms that cause the freshwater export to be concentrated in a series of discrete pulses during the fall/winter season. We find that the pulses occur once every 4.4 days on average and are associated with anticyclonic, surface-trapped eddies propagated through the strait by the mean outflow. Their occurrence is related to the passage of storms across Hudson Bay, although local instability processes also play a role in their formation. The eddies are responsible for approximately 40% of the mean volume transport and 50% of the mean freshwater transport out of the strait. We discuss the implications of this freshwater release mechanism on the delivery of nutrient-rich and highly stratified waters to the Labrador shelf, a productive region south of Hudson Strait.

© 2010 Elsevier B.V. All rights reserved.

1. Introduction

Observational efforts in the Arctic and subarctic seas have intensified in the last decade (e.g., Dickson et al., 2008), with the goal of obtaining baseline knowledge of the freshwater pathways in the high-latitude oceans. These efforts have resulted in more accurate and up-to-date estimates of the major freshwater budget terms (Serreze et al., 2006; Dickson et al., 2007), and, in some regions, led to new insights on the distribution and variability in freshwater storage.

One example is Hudson Strait, a 100 km wide, 400 km long channel with mean depths of ~300 m (Fig. 1) that connects Hudson Bay with the Labrador Sea. The Hudson Strait outflow is a baroclinic, buoyancy-driven current on the southern side of the channel (Fig. 1c), with a width of ~30 km and a depth of ~120 m (Straneo and Saucier, 2008a; Ingram and Prinsenberg, 1998; Drinkwater, 1988). The mean structure is primarily the result of the ~900 km³ yr⁻¹ river input into the Hudson Bay system (Déry et al., 2005) that sets up the buoyant current in roughly geostrophic balance (Straneo and Saucier, 2008a). In addition, the mean winds in the strait are downwelling favorable, which tends to steepen the current front and narrow the outflow against the Quebec coast, much like other coastal current systems (e.g., Lentz and Largier, 2006). The outflow represents the third largest net source of freshwater to the North Atlantic Ocean, behind only the flow through Fram and Davis Straits from the Arctic Ocean. The freshwater

transport exhibits a strong seasonal cycle, with increased discharge exiting through the Strait from October to April. The seasonality is due to the timing of river input into Hudson Bay, as well as the annual melt/freeze cycle of sea ice (Ingram and Prinsenberg, 1998; Straneo and Saucier, 2008b; Saucier et al., 2004).

A barotropic inflow brings Baffin Bay and Davis Strait water into the strait on the northern side, where it either re-circulates by mixing with the Hudson Strait outflow or passes into Hudson Bay itself, eventually exiting a few years later (Straneo and Saucier, 2008a; Saucier et al., 2004). The reprocessing and mixing of Davis Strait water with Hudson Strait water results in a mean freshwater transport of 78–88 mSv (2460–2780 km³ yr⁻¹), referenced to a salinity of 34.8 to compare with previous studies. This transport is approximately 50% of the total Labrador Current freshwater transport (Straneo and Saucier, 2008a,b).

In addition to its role in the high-latitude freshwater budget, the Hudson Strait outflow is also the primary conduit of high nutrient waters to the Labrador shelf. These nutrients are thought to greatly contribute to the high productivity and fish abundance over the Labrador shelf (e.g., Sutcliffe et al., 1983; Drinkwater and Harding, 2001).

Within the seasonal envelope of increased freshwater transport through the strait, observations display large variations in velocity and salinity on synoptic timescales of several days to a week (Straneo and Saucier, 2008a; Drinkwater, 1988). The main goal of the present work is to investigate these higher frequency, synoptic-scale variations in the Hudson Strait outflow, in contrast to previous work that focused on its mean and seasonal structure (Drinkwater, 1988; Straneo and Saucier,

* Corresponding author. Tel.: +1 206 221 4402.

E-mail address: dsuth@uw.edu (D.A. Sutherland).

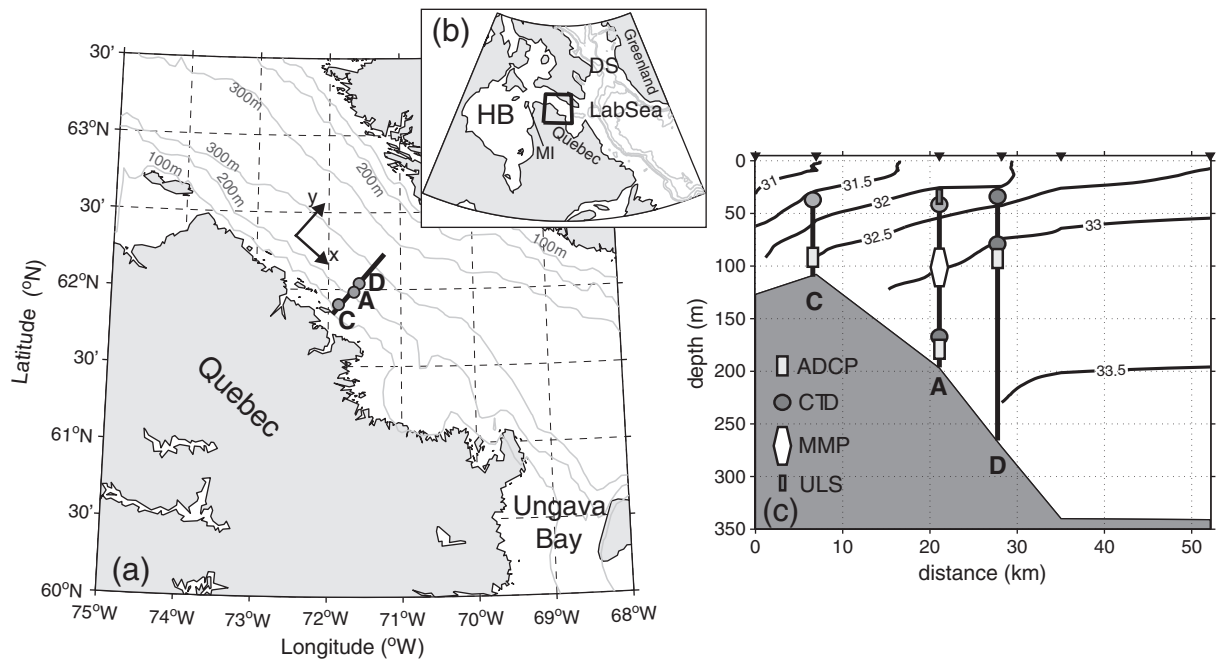


Fig. 1. (a) Mooring locations (C, A, and D) for the 2005–2006 deployment in the Hudson Strait outflow region. The solid line indicates the location of the CTD section displayed in c. (b) Regional map showing the location of Hudson Strait with respect to the larger Hudson Bay system (HB), the Labrador Sea, and Davis Strait (DS). The star marks the location of the wind data used for Hudson Bay, south of Mansel Island (MI). (c) Salinity section from a CTD transect (stations marked by black triangles) occupied in September 2005 along the line shown in a. Schematic representations of instrument depths and types are shown (MMP is McLane Moored Profiler, ULS is Upward Looking Sonar).

2008a,b). Using a set of moored observations across the strait over one year, we show that these high frequency events carry a significant fraction of the freshwater and volume transport of the Hudson Strait outflow. This puts into question the conventional view of the outflow as a continuous release of freshwater from Hudson Bay. Indeed, we propose that the mechanism for freshwater release from Hudson Bay is via a discrete series of pulses that carry low-salinity waters with a high river-water content through Hudson Strait. These pulses keep the Hudson Bay waters inside them weakly mixed, which has implications for the downstream stratification and productivity of the Labrador Current.

We do not ignore variability on shorter time scales, such as induced by tides, since tidal ranges in Hudson Strait can reach 8 m and play an important role in mixing (e.g., Egbert and Ray, 2001; Arbic et al., 2007), but we show that they do not control the variability observed on synoptic scales. A one-year long observational data set is outlined in Section 2. Analysis of this data is presented in Section 3, where we illustrate the freshwater transport mechanism that carries low-salinity pulses through the strait. The processes responsible for the formation and propagation of the low-salinity signals are discussed in Section 4.

2. Data

Three moorings were deployed in the outflow region of Hudson Strait from summer 2004 to summer 2007 and represent the first successful three-year mooring record from the strait (Fig. 1). Here we focus on the second deployment year, 2005–2006. Details of the processing, calibration, and mooring design for the first year, 2004–2005, can be found in Straneo and Saucier (2008a). Here we limit our analysis to the second year of data since it contains the only full depth and time record of hydrographic observations at the central mooring, velocity measurements across the mooring array, and additional instruments measuring fluorescence and sea ice draft (see following discussion). The spacing of the mooring array across the strait was changed from 2004 to 2005 to fully capture the outflow, which has a mean maximum velocity centered near mooring A, oriented at an

angle 125° along the bathymetry towards the southeast (Fig. 1a). The central mooring was also equipped with an Upward Looking Sonar (ULS) at 46 m depth that measured pressure, tilt, and sea ice draft (Straneo and Saucier, 2008a).

2.1. Velocity data and processing

Each mooring was equipped with an upward looking Acoustic Doppler Current Profiler (ADCP) situated near-bottom at mooring A (water depth ~171 m) and C (90 m), and at a depth of 77 m at mooring D (260 m), shown in Fig. 1c. The central mooring had a RDI 75 kHz long-range ADCP (10 m bins, 15 min. sampling), while the outer moorings were equipped with 300 kHz RDI sensors (4 m bins, 15 min. sampling). Velocities in the upper 20 m were blanked out at each location to reduce errors from surface effects, as well as to reduce impact of the large tidal range present (~8 m). Tidal velocities were estimated using the T-Tide package in MATLAB (Pawlowicz et al., 2002), and then subtracted out. The detided velocities were then filtered with a 34-h low-pass filter to remove any residual tidal signal. Adjustments were also made for the magnetic declinations of 29°W, 29.2°W, and 28.4°W for each ADCP at moorings A, D, and C, respectively.

Finally, the corrected, detided velocities were rotated into along- and across-strait directions using an angle of 125° (Fig. 1a). This angle was chosen as a mean bathymetric angle and corresponds well to the angle of maximum current variance observed, although each mooring location varied by several degrees around 125°. Throughout the rest of the paper, we refer to these processed, detided, and rotated velocities, U_{along} and U_{across} , simply as along- and across-strait velocities.

Data return from the ADCPs were good during 2005–2006, except at mooring A, where a software malfunction limited the data to a 4 month period, Sept. 10, 2005–Jan. 10, 2006. Along-strait velocities after the malfunction were estimated following the method of Straneo and Saucier (2008a). The missing velocity data (i.e., after Jan. 10, 2006) were reconstructed using an empirical relationship found between the ADCP velocity and the ULS tilt measurements during times when data were available. We emphasize though that these

velocities are not critical to the analysis presented here focusing on synoptic-scale variability mechanisms, since the majority of the events occur before the ADCP failure and that the conclusions do not depend upon the actual values calculated.

2.2. Hydrographic data and processing

Each mooring was equipped with a set of instruments to measure hydrographic properties (Fig. 1c). Mooring A was the most heavily instrumented, with an upper (46 m) and lower (171 m) Seabird SBE37 MicroCat conductivity, temperature, depth recorder (CTD) measuring salinity (S), temperature (T), and pressure at fixed locations, as well as a McLane Moored Profiler (MMP) that ranged from ~46 to 170 m along the mooring. The MMP collected profiles of S , T , pressure, and chromophoric dissolved organic matter (CDOM) fluorescence, at an average interval of every 4 h, while the CTDs recorded every 30 min. The outer mooring, D, also had an upper (27 m) and lower (77 m) CTD recording every 30 min. Unfortunately, the CTD placed on mooring C (41 m) failed, and no hydrographic data were recovered for this location during this year.

All of the CTDs were calibrated before deployment and post-recovery calibration was handled using hydrographic casts taken during the recovery, or by comparison to nearby instruments. The MMP data were interpolated to a regular grid in time (5 points per day) and in the vertical (2 m spacing). CTD data were subsampled in time to every hour to facilitate simpler data analysis. The MMP and CTD measurements of S and T at mooring A were combined to extend the vertical range of the observations to ~40–180 m (see Fig. 2).

In addition to the mooring data, hydrographic stations across the strait were occupied during each mooring deployment/recovery cruise, and provide snapshots of the outflow region (e.g., in September 2005 shown in Fig. 1c). For 2005, the observations were obtained using a 24-bottle rosette with a Seabird CTD on the Canadian Coast Guard vessel CCGS *Pierre Radisson*.

Meteorological variables over the strait and in eastern Hudson Bay were obtained from the six-hourly, $2.5^\circ \times 2.5^\circ$ resolution NCEP reanalysis fields (<http://www.cdc.noaa.gov/>). In particular, we used the 10-m zonal and meridional winds (U_{wind} , V_{wind}) interpolated to a position inside the strait near mooring A (61.98°N , 71.64°W) and over the entire Hudson Bay.

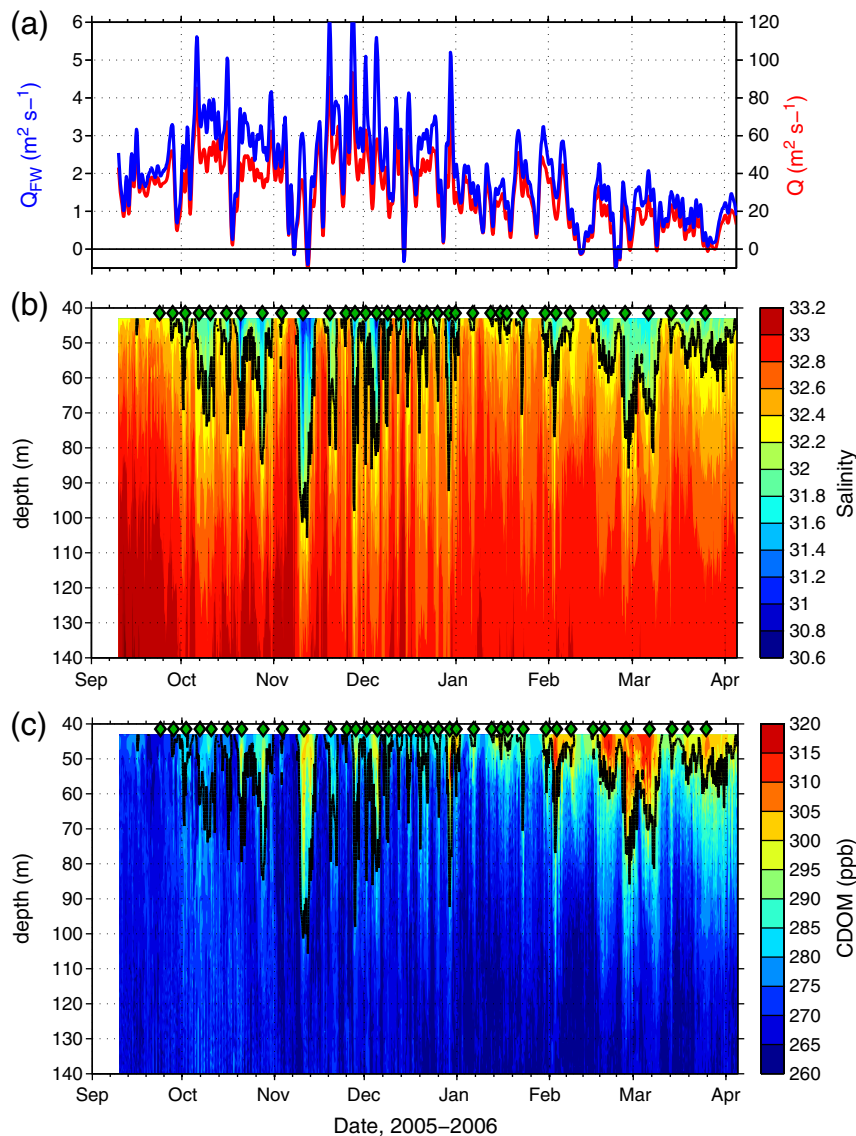


Fig. 2. (a) Observed freshwater transport (per unit width, relative to $S=34.8$, in blue) and volume transport (per unit width, red) of the Hudson Strait outflow, calculated at mooring A. (b) Salinity record from the moored profiler (MMP) at mooring A with the 32.2 isohaline contoured (black) and individual low-salinity events indicated (green diamonds). (c) Same as in b but for CDOM, with the 32.2 isohaline contoured (black).

3. Results

The salinity record from the MMP displayed in Fig. 2, combined with the snapshot of the outflow's cross-strait structure (Fig. 1c), illustrates several essential features of the Hudson Strait outflow. On seasonal timescales, the freshest waters ($S < 32.2$) leave Hudson Strait from early October to early January, with additional low-salinity water observed from February to April. However, this secondary pulse is less pronounced in the freshwater transport calculation since it is associated with relatively weak velocities (Fig. 2).

On synoptic timescales within this seasonal envelope, the dominant feature in the salinity record is a series of low-salinity pulses lasting from one to several days (Fig. 2b). These low-salinity pulses reach depths of 100 m. Note that the CTD section shown in Fig. 1c indicates a depth for the 32.2 isohaline at mooring A of roughly 50 m, which is relatively shallow in the context of the yearly salinity record. The CTD section illustrates the cross-strait salinity gradient, $\partial S / \partial y > 0$, that is persistent throughout the year between moorings A and D, but unknown between A and C for 2005–2006 since the CTD instrument failed at the inner mooring. Data from a 2004 hydrographic section in the same region show that $\partial S / \partial y$ is positive across the outflow and intensified in the surface layer, in accordance with the baroclinic nature of the flow (Straneo and Saucier, 2008a).

The record of CDOM throughout the water column at mooring A (Fig. 2c) shows a similar seasonal and high frequency variability to the salinity observations. High CDOM corresponds to high river water content, but can be modified by the seasonal sea ice cycle. The highest values of CDOM are confined in time and in the vertical to the freshest salinities, as the 32.2 isohaline captures them qualitatively well (Fig. 2c).

The freshwater and volume transports calculated at mooring A (Fig. 2a), referenced to a salinity of 34.8, show considerable variability on similar synoptic time scales as the salinity variability. The range of freshwater transport per unit width goes from a minimum just below zero to a maximum near $6 \text{ m}^2 \text{ s}^{-1}$. Transports were calculated using a constant salinity above the shallowest recorded value at 46 m, and constant velocity above the shallowest ADCP bin at 20 m. These assumptions most likely result in underestimates of the volume and freshwater transports at mooring A (Straneo and Saucier, 2008a), but we emphasize that the variability is what is important to this study and not the exact values.

The extremes in freshwater transport seem to be related to the occurrence of low-salinity events observed by the MMP at mooring A. Thus, to understand what controls the freshwater transport variability, we need to understand the processes behind the synoptic scale variability.

3.1. Synoptic-scale variability

Fig. 3 displays a zoom-in of observations taken at mooring A, with S , T , and CDOM from the MMP, and U_{across} from the ADCP, during a 6-day period in late October 2005. The salinity data (Fig. 3a) show the appearance of low-salinity waters with $S < 31.5$ centered near 28-Oct-2005, when the 32.5 isohaline dips to ~105 m. After this maximum depth is reached, the isohalines shoal and return to their previous vertical positions. Associated with the presence of the relatively fresh, upper-layer water is relatively high T (Fig. 3b), high CDOM (Fig. 3c), and a reversal in U_{across} from onshore to offshore-directed velocity (Fig. 3d). We define the passage of an event occurring when a local minimum in S is reached in the upper water

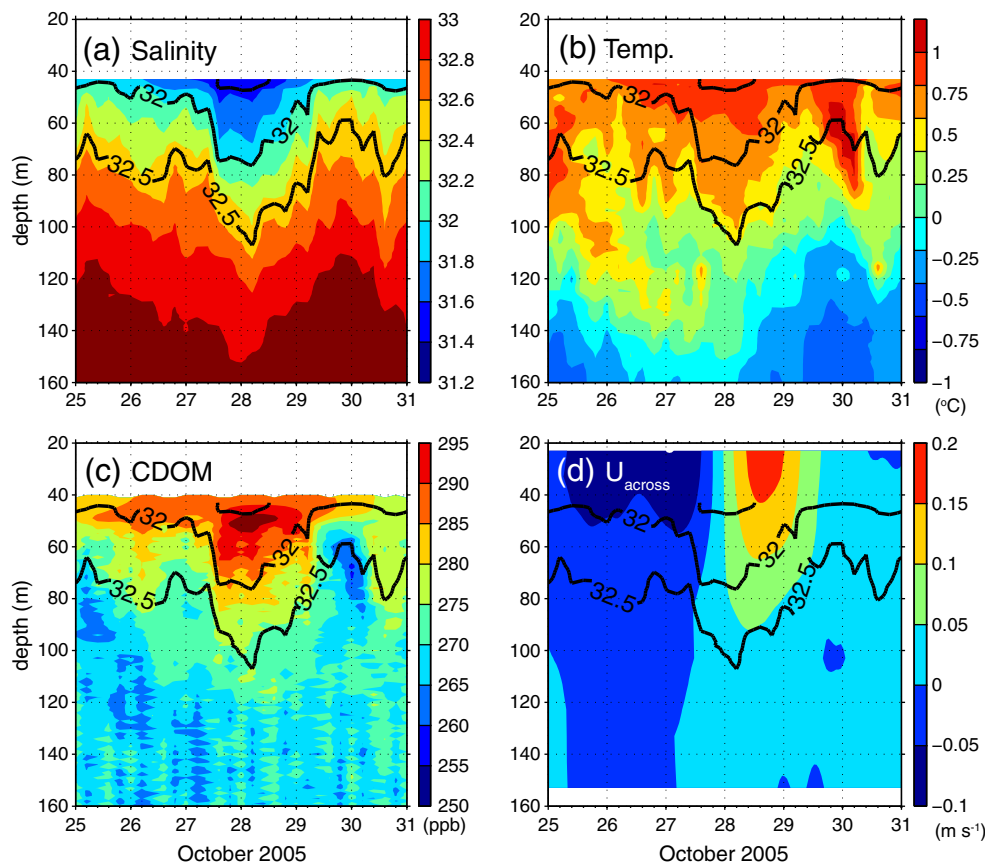


Fig. 3. (a) Observed salinity record from the moored profiler (MMP) at mooring A during a typical low-salinity event that occurred in late October 2005. Select isohalines (black lines: 31.5, 32, and 32.5) are indicated similarly across all panels. (b) Same as in a, but for the observed temperature record from the MMP. (c) Same as in a, but for the observed CDOM record from the MMP fluorometer. (d) Across-strait velocity ($U_{\text{across}} < 0$ is onshore) for the same time period as in a–c, from the ADCP at mooring A.

column (~40–60 m) and is coincident with a zero crossing in U_{across} in the same depth range.

Using this definition for a low-salinity event results in 38 identifiable pulses from late September 2005 to early April 2006 (Fig. 2b). Since S varies seasonally, using a local minimum criterion combined with a velocity criterion gave more meaningful results than using a fixed salinity level. Although T and CDOM were not used in defining when an event occurred, they were coherent with the S and U_{across} signals (Fig. 3) in each identified pulse. On the other hand, observations of U_{along} and MMP backscatter (not shown) did not show a consistent signal associated with the occurrence of these low-salinity events. In general there was an increase in U_{along} associated with each event, but the peak increase did not always exactly match the timing of the minimum salinity.

The occurrence of these low-salinity pulses was also observed in the sea ice data from the ULS located on the central mooring (Fig. 4). Ice covers Hudson Strait from early winter to spring (Dec–Apr). Throughout the fall months, large pieces of sea ice from northern Hudson Bay, such as Foxe Basin, can be observed in the strait outflow (Gagnon and Gough, 2005). The pulses are not associated with these pieces of sea ice, but are, instead, associated with minima in sea-ice draft. A correlation of the upper water column salinity (as a proxy for the low-salinity events) and the maximum ice thickness results in a positive correlation coefficient of 0.35, which is significant at the 95% level based on $N' - 2$ where N' is the e -folding value of the autocovariance of the observed variable (Emery and Thomson, 1997). The relationship between the ice draft and the pulses is discussed further in Section 4.

Two mechanisms could explain the propagation of low-salinity water past mooring A in what appears to be a series of pulses, as well as explain the variations in freshwater transport. Variations caused by the movement of the outflow frontal region back and forth across mooring A (i.e., imagine the 32 isohaline in Fig. 1c oscillating left to right across the mooring) can be dismissed as the cause due to the observed reversal in U_{across} from onshore to offshore-directed velocity. This is supported by a simple salt balance discussed in Section 4.

The first plausible explanation is that these pulses are due to the freshwater input from different sources both spatially and temporally separated, either caused by wind-induced accelerations of the boundary current in Hudson Bay (Prinsenberg, 1987) or by individual river plumes making their way into the Strait. These pulses would show up in the strait as buoyant, anticyclonic eddies propagating by the mooring array. The second mechanism, inherent to the outflow current itself, is that local baroclinic or barotropic instabilities cause the outflow to go unstable and break up into a series of finite low-salinity eddies that then propagate by the moorings.

To investigate these possible mechanisms, we next examine the velocity and salinity structure of an event from data taken across the mooring array. The U_{across} and U_{along} velocities for the late October event, averaged over the upper 60 m, are displayed in Fig. 5. At the two outer moorings (A and D, Fig. 1), the signal in U_{across} is similar, showing a switch from onshore to offshore flow (Fig. 5a–b). At the inner mooring C, on the other hand, the signal is reversed with offshore flow preceding onshore flow. The zero-crossing of all three U_{across} signals occur at approximately the same time. For U_{along} , the observations at moorings A and D are again comparable, with an increase coincident with the switching from onshore to offshore flow, though the exact timing does not agree as well as for U_{across} . Inshore at mooring C, the velocity is upstrait during the event (Fig. 5c).

Alongside the observed velocities are velocities derived from a simple two-layer eddy model with a core speed of 0.15 m s^{-1} and a radius of 20 km, corresponding to a passage timescale of ~1.5 days. This model assumes the eddy can be idealized as a Rankine vortex that has a solid-body core within a radius R and $1/r$ decay elsewhere, where r is the azimuthal position along the eddy radius (Fig. 6). A similar model was used in the Labrador Sea to investigate eddies observed by a single mooring (Lilly and Rhines, 2002). As an eddy propagates by the mooring array, the velocities are taken from the slice that each mooring would measure. For example, imagine an anticyclonic, surface-trapped eddy propagating through Hudson Strait such that the center of the eddy passed just south of mooring A ($r < R$), while mooring D observed the region just north of the eddy edge ($r > R$), and mooring C observed just south of the eddy edge ($r > R$). Fig. 6 presents a schematic of this situation. The resulting velocities at each mooring would be those illustrated in Fig. 5, which compare reasonably well to the observed velocities.

Hodographs of the same data are revealing when plotted with concurrent salinity data from the upper CTDs where available for moorings A and D (Fig. 5d–f). The eddy core appears as a straight line in the theoretical hodograph (Fig. 5d), and the observations show a similar straight-line feature that corresponds to the observed low-salinity water. The observations are consistent at mooring D (Fig. 5e), which shows that the hodograph should be circular for a slice north of the eddy center and that compares well to the observed velocities and low-salinity water. The circle is reversed at mooring C (Fig. 5f), as the inner mooring observes an eddy slice south of the edge and measures oppositely directed flow.

All 38 of the identifiable events from Sept. 2005 to Apr. 2006 had a velocity structure qualitatively consistent with the observations shown in Fig. 5. This suggests that these events are anticyclonic eddies with a low-salinity, buoyant core.

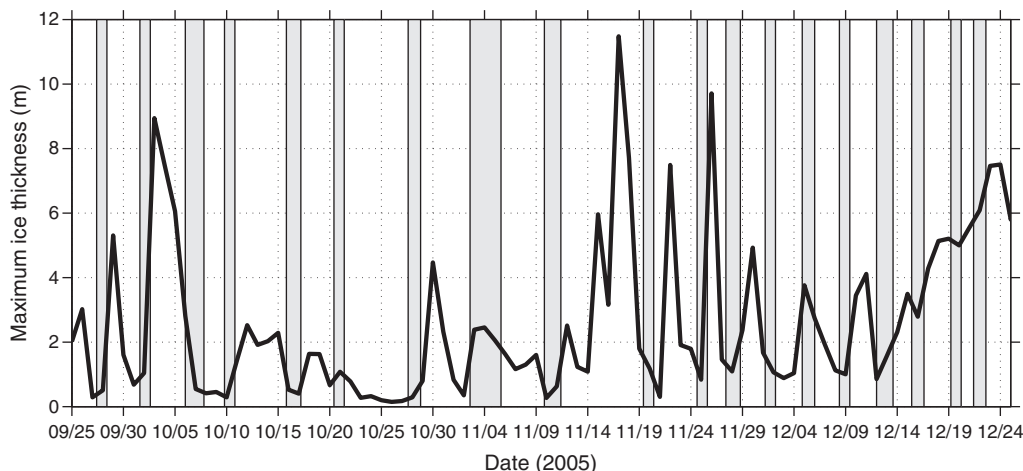


Fig. 4. Time-series of daily maximum ice draft (m) measured by the Upward Looking Sonar instrument on the center mooring during a three-month period of fall 2005. Shading indicates occurrences of low-salinity pulses observed by the mooring array.

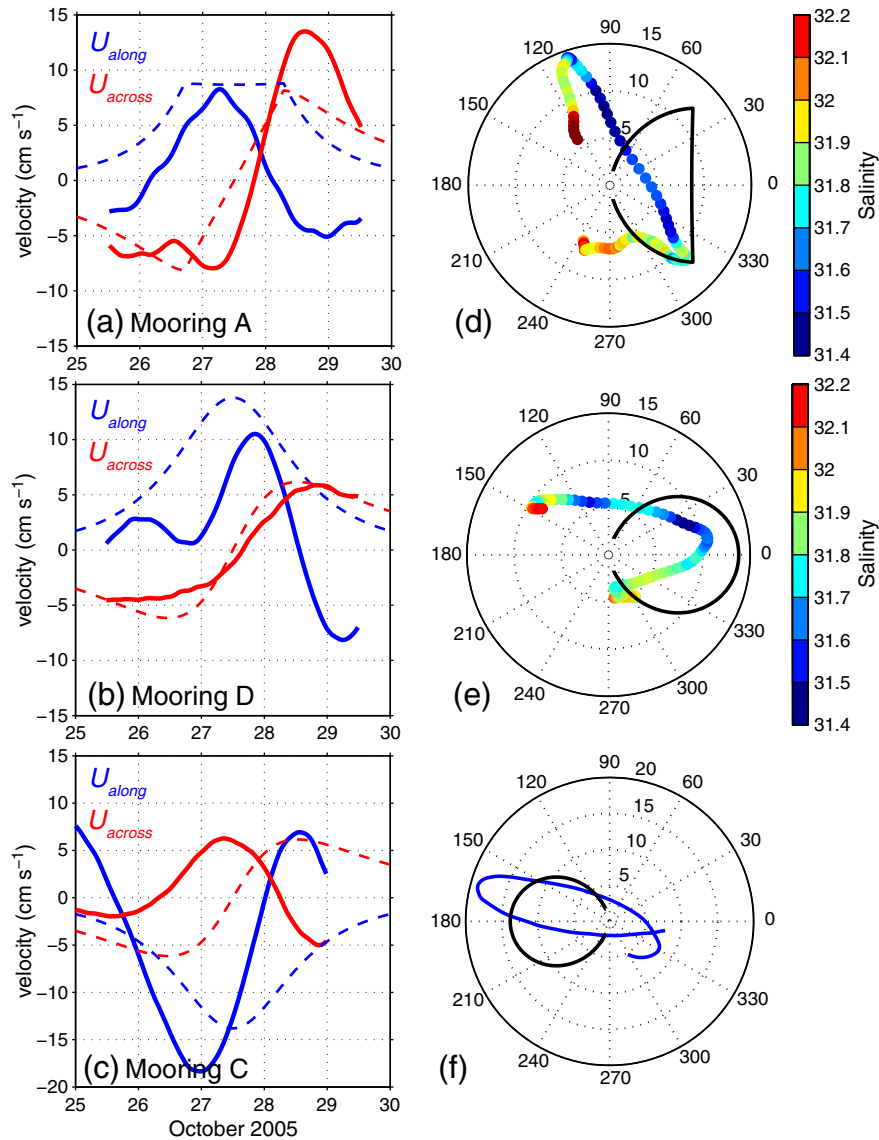


Fig. 5. (a) Observed upper layer (0–60 m) velocities (solid lines) at the central mooring for a typical low-salinity event, compared to theoretical velocities (dashed lines) taken from slicing through a two-layer eddy north of the eddy center. (b) Same as in a, but for mooring D with the slice north of the eddy edge. (c) Same as in a, but for mooring C with the slice south of the eddy edge. (d) Hodograph of the observed velocities in a colored with the salinity at the upper CTD, plotted against the theoretical velocities in a (black line). (e) Same as in d, but for mooring D. (f) Same as in d, but for mooring C, where no salinity data was available.

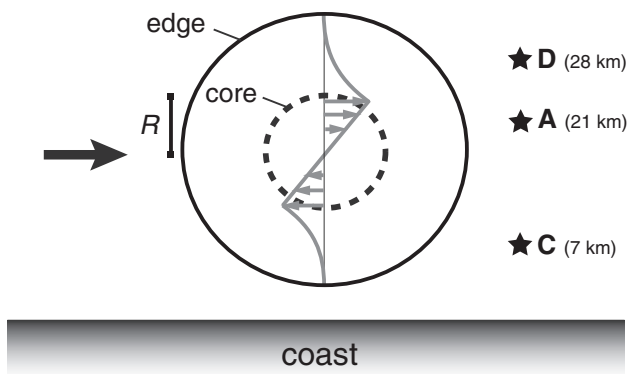


Fig. 6. Schematic of an anticyclonic, low-salinity eddy propagating by the mooring array (shown to approximate scale, with distances of each mooring given from the coast). The eddy has a core of radius R (dashed circle), a fresh anomaly out to its edge (solid circle), and is moving from left to right. Gray lines show the velocity structure of an ideal Rankine vortex.

In addition to the consistent hydrographic and CDOM properties observed during each eddy, the stratification, $N = (-g/\rho_0 \cdot \partial\rho/\partial z)^{1/2}$ in cycles per hour (cph), of the outflow was higher at depth during times when an eddy was present and propagating by the mooring array. Fig. 7a shows the stratification during the same late October event. Stratification increased in deeper water (~60–120 m range) as the eddy propagated by, and closely matched the salinity contours, but was decreased in the surface core. On the outer edges of the eddy, the gradients were intensified and the highest stratification was observed in the surface waters. The mean stratification over the depth range 60–120 m during the high freshwater transport season (Oct–Jan) was 0.093 cph, while the mean taken over just the times when an eddy was present equaled 0.12 cph (with a standard error, $\sigma = 0.006$, corresponding to 38 events). This stratification anomaly is associated with the hydrographic signal of each low-salinity pulse, which on average over the same depth range (60–120 m), had a salinity anomaly of -0.13 ($\sigma = 0.02$) from the mean S of 32.4, a temperature anomaly of 0.012 ($\sigma = 0.01$) from the mean $T = -0.63$ °C, and a high CDOM anomaly of 8.8 ppb ($\sigma = 1.7$) over the mean of 280 ppb.

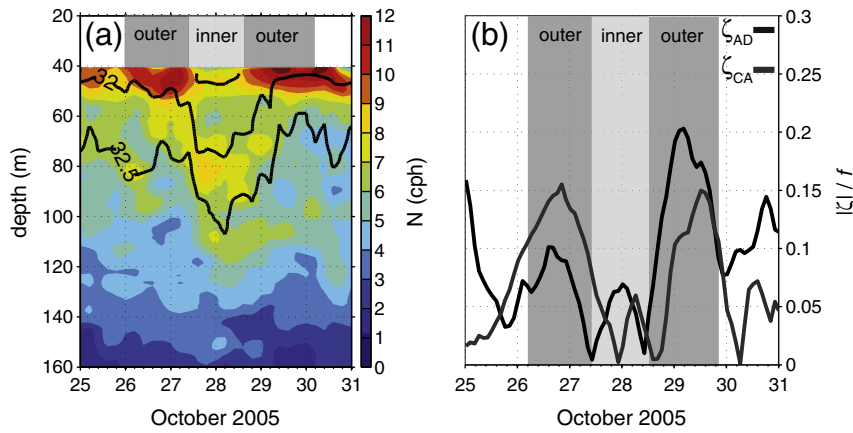


Fig. 7. (a) Observed stratification from the moored profiler (MMP) at mooring A during a typical low-salinity event that occurred in Oct. 2005, with the inner core of the eddy differentiated from the outer core (shading). Select isohalines (black lines: 31.5, 32, and 32.5) are indicated similarly across all panels. (b) The absolute value of estimated relative vorticity, ζ , versus time, calculated between moorings A–D (black) and moorings C–A (gray). ζ is scaled by the Coriolis parameter, f . Shading corresponds to the distinct eddy regions shown in a.

Using the velocity data from the three moorings, we can also estimate the importance of the relative vorticity, $\zeta = -\partial U_{\text{across}}/\partial y + \partial U_{\text{along}}/\partial x$, where x, y are the along- and across-strait coordinates, respectively. Taking the ratio $|\zeta|/f$ gives a useful measure of the nonlinearity of the flow. We estimate the $\partial U_{\text{across}}/\partial y$ term directly from the ADCP data at the three moorings, averaged over the upper 80 m in order to use the same depths from all three moorings. The $\partial U_{\text{along}}/\partial x$ term we calculated from the along strait velocities measured at each mooring averaged over the upper 80 m, and first found $\partial U_{\text{along}}/\partial t$. To convert from ∂t to ∂x , we assumed that the velocity anomalies (i.e., the eddies) were propagated past the mooring array by a slowly-varying background flow equal to a low-pass filtered U_{along} , calculated using a 7-day Hanning window. The along-strait term was always smaller than the cross-strait term, so the changes to ζ due to the aforementioned assumptions were not substantial.

Relative vorticity is seen to be significant around the outer core of the eddy, with the maximum ratio $|\zeta|/f = 0.2$ (Fig. 7b). Over the entire fall freshwater season, these ratios ranged from 0 to 0.45, with the highest values occurring in the intense gradients observed in the outer core of each eddy.

Over the eight month period investigated, the mean vertical extent of the 38 events, defined by the 32.2 isohaline, was ~ 75 m ($\sigma = 10$ m), with one event occurring every 4.4 days on average. The mean eddy velocity was ~ 0.19 m s $^{-1}$ ($\sigma = 0.08$ m s $^{-1}$ with a large seasonal cycle), calculated as the difference between U_{along} measured at the center of each event at mooring A and the 30-day low-pass filtered U_{along} . Using this velocity scale, we calculated the horizontal extent of each event by converting time into distance. The mean horizontal radius was ~ 25 km ($\sigma = 12$ km). This scale is about $3.5L_d$, where $L_d = (g'h)^{1/2}/f$ is the Rossby radius of deformation based on the mean reduced gravity g' and mean vertical extent h . The mean g' was 0.011 m s $^{-2}$ ($\sigma = 0.003$ m s $^{-2}$) and was calculated using $g' = g\Delta\rho/\rho_0$, where $\Delta\rho$ is the difference between density measured at the upper and lower CTDs at mooring A, and $\rho_0 = 1025$ kg m $^{-3}$.

The effect of the eddies on the freshwater and volume transports of the outflow is significant. If we assume that the outflow velocity is coherent across the mooring array, as observed during 2004–2005 (Straneo and Saucier, 2008a), then we can take the transports calculated at mooring A (Fig. 2a) as a proxy for the entire outflow transports. Removing the time periods when eddies were present results in drastically reduced transport numbers: the volume transport carried by the eddies is 40% of the total, while the freshwater transport contribution is 50% of the total.

4. Origin of the eddies

The observations displayed in Figs. 3–7 suggest that the synoptic scale variability dominating the MMP salinity record (Fig. 2a) is due to a series of anticyclonic, surface trapped eddies propagating by the mooring array. The frontal movement mechanism would produce a velocity signal in the opposite sense to what is observed at moorings A and D. To test this further, we can calculate the terms in a simple salt balance,

$$S_t + U_{\text{across}}S_y + U_{\text{along}}S_x = 0 \quad (1)$$

where subscripts denote partial differentiation in time (t) and in the across- (y) and along- (x) strait directions. Eq. (1) is derived assuming that the vertical velocity, W , equals zero.

If the variability was due to movement of the outflow frontal region back and forth across the mooring array, the first two terms in Eq. (1) would roughly balance. We can calculate the time rate of change of salinity (S_t) and the across-strait advective term ($U_{\text{across}}S_y$) directly from the mooring observations. To do this, we use the observed salinity at 45 m depth at mooring A for S . To calculate the advective term, we use U_{across} at 45 m from mooring A, while the cross-strait salinity gradient is estimated as the difference between the salinity at mooring A at 45 m and that at mooring D. Since there was no instrument at 45 m depth at mooring D, we linearly interpolated between the upper and lower CTDs that were present. The along-strait advective term can only be estimated as a residual between the other two terms.

The results of estimating these salt budget terms are shown in Fig. 8 for the first half of the 2005–2006 mooring deployment. The timing of each event is marked by an open circle, which corresponds to the zero-crossing of S_t as the observed salinity first decreases, then increases. The across-strait advective term is, as expected, in the opposite sense to what is needed to balance S_t , indicating that frontal movements are not responsible for the observed variability. This implies that the along-strait advective term must be large enough to balance the residual.

By eliminating the frontal movement mechanism, we are left with either the remotely forced mechanism, through wind events or individual river discharge events, or the local instability mechanism, to explain the variability in the Hudson Strait outflow. Previous studies in Hudson Bay have shown the cyclonic boundary current there to vary synoptically with the passage of storms over the region,

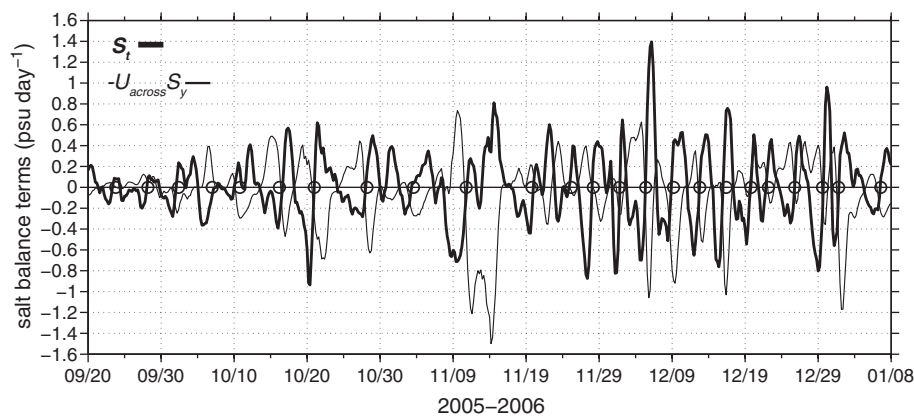


Fig. 8. Two terms (S_t : rate of change of salt, $-U_{\text{across}}S_y$: cross-strait advective term) of a simple salt balance calculated at the central mooring at 45 m depth. The along-strait advective term could not be estimated from the data. Observed low-salinity events are indicated with open circles.

suggesting it is wind-driven (Prinsenberg, 1987; Saucier et al., 2004). The modeling study by Saucier et al. (2004) suggested that the head region of Hudson Strait where Hudson Bay, Foxe Basin, and the strait meet, is a region of intense eddy features and complicated circulation patterns. In particular, they noted that flow through the constriction between Mansel Island and Quebec would stop and go periodically, presumably due to the acceleration of the boundary current to the south. Periodic flow through this gap could generate the anticyclonic, buoyant eddies observed downstream in the Hudson Strait outflow as the cyclonic Hudson Bay boundary current exits into the Strait and turns right under the effects of rotation and buoyancy. The minima in ice draft associated with the majority of the eddies (Fig. 4) support this hypothesis as well, since waters exiting from southern Hudson Bay during the fall months would tend not to have sea ice cover, as opposed to a more northern origin (e.g., Foxe Basin).

To test this hypothesis, we constructed a time series of wind stress curl, $\text{curl}_z\tau$, over Hudson Bay to serve as a proxy for the acceleration of the boundary current due to the passage of storms across Hudson Bay. As low-pressure systems move across the bay, positive curl accelerates the boundary current on the eastern side of the bay due to northward winds in that region (Prinsenberg, 1987; Saucier et al., 2004). At some later time period, the accelerated flow generated by this positive curl moves past Mansel Island and into Hudson Strait to be observed by the mooring array. Support for this process is shown in Fig. 9a, which compares the time series of $\text{curl}_z\tau$ with a calculation of freshwater flux from historical mooring data located near Mansel Island in the boundary current (Fig. 1). The data come from a yearlong mooring deployment conducted by the Department of Fisheries and Oceans, Canada in 1992–1993 (Saucier et al., 1994). The mooring had a current meter and CTD sensor positioned at 28 m depth, in a total water depth of ~75 m. The freshwater flux time series in Fig. 9a is calculated using the low-pass filtered (34-h Hanning window) along-channel velocity (approximately northwestward) and the salinity observations collected at the same time. Maximum correlation between the time series was found to be $R=0.55$ (significant at the 95% level) with $\text{curl}_z\tau$ leading the freshwater flux by 1.5 days.

Based on this relationship between freshwater flux and wind stress in Hudson Bay, one might expect there to be a similar relationship inside Hudson Strait, but with a longer lag time. We can test this using the mooring data from 2005 to 2006 and the low-pass filtered $\text{curl}_z\tau$ obtained from the NCEP wind fields averaged over the entire Hudson Bay region during the same time period (Fig. 9b). Squares indicate the lagged time that a low-salinity event was observed to pass by the mooring array. Estimates of the lag time were calculated using the observed along-strait velocity at mooring A over the upper 60 m and a length scale of 310 km that is roughly the distance from the head of Hudson Strait to the mooring array. The

velocities used were low-pass filtered with a running 3-day average to remove the effects of the eddy itself and use the speed at which the eddy was propagating at in the outflow current. These lag times ranged from 10 to 14 days, with the longer times associated with Jan–Apr as the outflow slowed down.

The lagged pulses were correlated with a positive curl, i.e., northward wind acceleration in eastern Hudson Bay. Using the appropriate lag time, 34 of the 38 identified low-salinity events observed at the mooring array corresponded to an increase in northward winds in eastern Hudson Bay. This result strongly supports the notion that the passage of storms over Hudson Bay and the resulting acceleration of the boundary current there are related to the generation of buoyant eddies that are exported to Hudson Strait. We attribute the discrepancy in the remaining 4 events to either to a

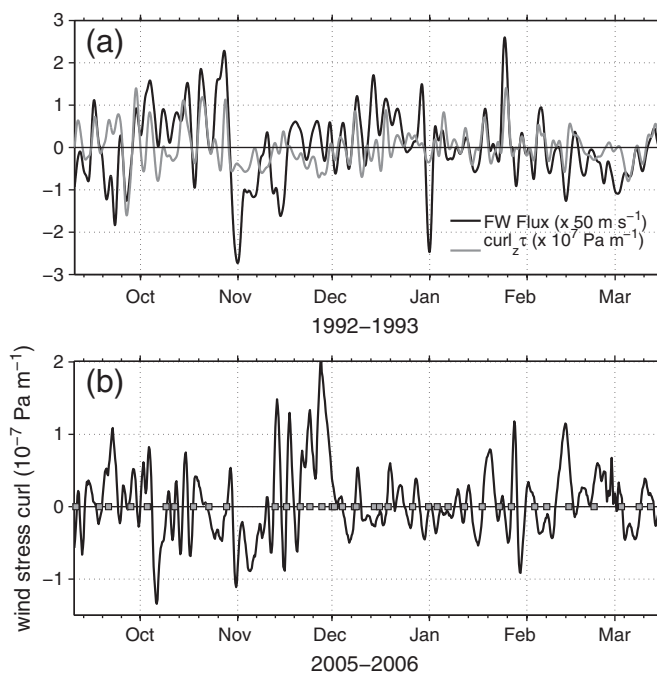


Fig. 9. (a) Time series of wind stress curl, $\text{curl}_z\tau$ ($\times 10^7 \text{ Pa m}^{-1}$), averaged over Hudson Bay and the freshwater flux ($\times 50 \text{ m s}^{-1}$) calculated from the DFO mooring in 1992–1993. The freshwater flux estimate is lagged by 1.5 days to show the maximum correlation between the time series. (b) Wind stress curl, $\text{curl}_z\tau$ ($\times 10^{-7} \text{ Pa m}^{-1}$), averaged over Hudson Bay calculated from the NCEP reanalysis data for 2005–2006. The timing of low-salinity events observed propagating by the mooring array are shown (gray squares) lagged by the product of their along-strait speed and the distance to the western entrance of Hudson Strait (~310 km).

difference in origin for the low-salinity waters, i.e. Foxe Basin, which would change the timing of the wind correlation, or to a difference in mechanism, such as a more local eddy generation that would have no correlation with the wind.

Winds in Hudson Bay are correlated to the winds inside the strait, however, so we also tested the relationship between the local wind forcing and the observed velocities in the outflow. Table 1 lists the results of these correlations for U_{along} and U_{across} measured at 45 m at each mooring against V_{wind} . In this case, V_{wind} is taken at a location inside the strait near mooring A at 71.3°W, 61.9°N. Significant correlations (95% level) were found only at the shallow inner mooring, with maximum correlations in the velocity occurring at a lag of 1 day to the wind forcing. Since no significant correlations were found at moorings A and D, this suggests that local wind forcing is not the cause of the observed velocity fluctuations.

Of the remaining oceanographic processes that could explain the observed synoptic scale variability, the individual river plume mechanism is easiest to dismiss. Rivers certainly play a role in supplying the freshwater for these events and can have strong freshets that are relatively short-lived. Model results and previous field efforts inside Hudson Bay, though, show the boundary current to be mixed enough that the distinct rivers feeding the current are lost (Ingram and Prinsenberg, 1998; Saucier et al., 2004; St-Laurent et al., 2011). The properties of the outflow, with low salinities and high CDOM suggest that the water has a partly riverine origin, but identifying discrete river freshets would be impossible.

The strongly baroclinic velocity and buoyancy signature of the outflow does raise the possibility that local instability processes could be a cause for the observed variability. This mechanism is in contrast to eddies being formed at the entrance to Hudson Strait, which can be thought of as a remote instability mechanism forced by the wind. The baroclinic and barotropic instability mechanisms are difficult to diagnose with limited observations, although many coastal currents previously studied, such as the Norwegian Coastal Current (Mork, 1981), the East Greenland Coastal Current (Sutherland and Pickart, 2008), the flow off Cape Cod, USA (Shcherbina and Gawarkiewicz, 2008) and the western Arctic shelfbreak current (Spall et al., 2008) have been observed to show variations associated with baroclinic instabilities. Theoretical scales can be estimated from the limited hydrographic section data to constrain the growth rates and corresponding horizontal scales of the baroclinic instability process.

For example, the slope Burger number, $Sl = \alpha N/f$, where α is the bathymetric slope is a measure of the buoyant current structure, with $Sl \ll 1$ indicating a slope-controlled regime and $Sl \gg 1$ indicating a surface-trapped current (Lentz and Helfrich, 2002). Taking typical values for the Hudson Strait outflow, $\alpha = 0.01$, $f = 1.3 \times 10^{-4} \text{ s}^{-1}$, and a stratification range of $N = 0.0066\text{--}0.010 \text{ s}^{-1}$, gives $Sl \sim 0.5\text{--}0.7$, suggesting the outflow is in the slope-controlled regime of buoyant currents. Slope-controlled currents tend to be more stable than buoyant currents against a vertical wall (Lentz and Helfrich, 2002). A related parameter to investigate this stability is $\delta = \alpha/\partial\rho/\partial z$, the ratio of the bottom slope to the isopycnal slope. Typically, $\delta < 0$ for buoyant currents (Shcherbina and Gawarkiewicz, 2008; Blumsack and Gierasch, 1972). For Hudson Strait, given the typical bottom slope, $\alpha = 0.01$, and an isopycnal slope estimated from hydrography using

the 32 isohaline (Fig. 1c), $\delta \approx -2$. Given δ , we can estimate the maximum growth rate and length scale of baroclinic instability (following equations 3.12 and 3.13 of Blumsack and Gierasch, 1972; Shcherbina and Gawarkiewicz, 2008), which are 5.8 days^{-1} and 2.0 km, respectively. The length scale corresponds to a wavelength of $2\pi \cdot 2.0 \text{ km}$, 12.9 km, which is $\sim 1.6L_d$. Thus, the range of scales due to a baroclinic instability mechanism is plausible given the observed scales of the eddies, but a detailed stability analysis and discussion of the instabilities is beyond the scope of this paper.

5. Conclusions and summary

The series of discrete, low-salinity pulses observed in the Hudson Strait outflow are surface-trapped, anticyclonic eddies with vertically and horizontally coherent salinity, CDOM, and velocity signals. These eddies carry approximately half of the freshwater transport and 40% of the volume transport through Hudson Strait. This is an important result as it represents a form of freshwater transport contrary to the conventional view of a continuous coastal current outflow from Hudson Bay. Since the freshwater outflow modulates how high-stratification and high-nutrient water enters the northern North Atlantic, the fact that the outflow is confined to coherent eddy-like structures that preserve their properties for longer periods of time is a critical point. Water masses carried inside these features will be less mixed, and the nutrients they bring from rivers, as well as any pollutants, will enter Hudson Strait and the Labrador shelf higher in the water column.

We find that the timing of these eddies can be explained by atmospheric variability over Hudson Bay, due to the passage of storms over the bay that force low-salinity boundary current waters out near Mansel Island. Whether or not the inflow on the northern side of the strait exhibits similar synoptic variability, or is influenced by the propagation of these eddies in the outflow, remains an open question. Another uncertainty is what the spatial and temporal along-strait variations in salinity are in Hudson Strait. Observational efforts are underway to explore the first question, with moorings placed in the northern Strait in 2009. However, models may provide the most useful insight into quantifying the along-strait variability, though they must be of high enough resolution to resolve the mesoscale features we observe.

Acknowledgments

This work was funded by the National Science Foundation grant OCE-0751554, with additional funding from the Office of Naval Research grant N00014-08-10490. Special gratitude to Jim Ryder, the Canadian Coast Guard ships and crew who helped deploy and recover the moorings in Hudson Strait. The authors also thank Emmanuel Boss for insights on the CDOM data, and Andrey Shcherbina and Rocky Geyer for useful comments. Two reviewers provided useful comments and suggestions that improved the clarity and content of the paper.

References

- Arbic, B.K., St-Laurent, P., Sutherland, G., Garrett, C., 2007. On the resonance and influence of the tides in Ungava Bay and Hudson Strait. *Geophys. Res. Lett.* 34. doi:10.1029/2007GL030845.
- Blumsack, S.L., Gierasch, P.J., 1972. Mars: the effects of topography on baroclinic instability. *J. Atmos. Sci.* 29, 1081–1089.
- Déry, S.J., Stieglitz, M., McKenna, E.C., Wood, E.F., 2005. Characteristics and trends of river discharge into Hudson, James, and Ungava bays, 1964–2000. *J. Climate* 18, 2550–2557.
- Dickson, R., Rudels, B., Dye, S., Karcher, M., Meincke, J., Yashayaev, I., 2007. Current estimates of freshwater flux through Arctic and subarctic seas. *Prog. Oceanogr.* 73, 210–230.
- Dickson, R., Meincke, J., Rhines, P.B., 2008. Arctic–Subarctic Ocean Fluxes: Defining the Role of the Northern Seas in Climate. Springer, 738 pp.
- Drinkwater, K.F., 1988. On the mean and tidal currents in Hudson Strait. *Atmos. Ocean* 26, 252–266.

Table 1

Correlations of the along-strait wind obtained from NCEP with the observed upper layer along- and across-strait velocities (45 m) at the three moorings deployed in 2005–2006. Significant correlations ($p < 0.05$) are shown in bold. In parentheses is the lag that corresponds to the maximum correlation when it was significant, otherwise, no significant correlations were found and the coefficients are for zero lag.

	Mooring C	Mooring A	Mooring D
U_{along}	0.61 (1 day)	0.05	0.01
U_{across}	−0.35 (1 day)	0.15	−0.06

- Drinkwater, K.F., Harding, G.C., 2001. Effects of the Hudson Strait outflow on the biology of the Labrador Shelf. *Can. J. Fish. Aquat. Sci.* 58, 171–184.
- Egbert, G.D., Ray, R.D., 2001. Estimates of M_2 tidal energy dissipation from TOPEX/Poseidon altimeter data. *J. Geophys. Res.* 106, 22,475–22,502.
- Emery, W.J., Thomson, R.E., 1997. *Data Analysis Methods in Physical Oceanography*. Pergamon Press, 634 pp.
- Gagnon, A.S., Gough, W.A., 2005. Trends in the dates of freeze-up and breakup over Hudson Bay, Canada. *Arctic* 58, 370–382.
- Ingram, R.G., Prinsenberg, S.J., 1998. Coastal oceanography of Hudson Bay and surrounding Eastern Canadian Arctic waters. *The Global Coastal Ocean, Regional Studies and Synthesis*. In: Robinson, Brink (Eds.), *The Sea*, Vol. 11, pp. 835–861.
- Lentz, S.J., Helfrich, K.R., 2002. Buoyant gravity currents along a sloping bottom in a rotating fluid. *J. Fluid Mechanics* 464, 251–278.
- Lentz, S.J., Largier, J., 2006. The influence of wind forcing on the Chesapeake Bay buoyant coastal current. *J. Phys. Oceanogr.* 36, 1305–1316.
- Lilly, J.M., Rhines, P.B., 2002. Coherent eddies in the Labrador Sea observed from a mooring. *J. Phys. Oceanogr.* 32, 585–598.
- Mork, M., 1981. Circulation phenomena and frontal dynamics of the Norwegian Coastal Current. *Phil. Trans. R. Soc. Lond. Ser. A* 302, 635–647.
- Pawlowicz, R., Beardsley, R., Lentz, S., 2002. Classical tidal harmonic analysis including error estimates in MATLAB using T_TIDE. *Comput. Geosci.* 28, 929–937.
- Prinsenberg, S.J., 1987. Seasonal current variations observed in western Hudson Bay. *J. Geophys. Res.* 92, 10,756–10,766.
- Saucier, F.J., Larouche, P., Dionne, J., 1994. Moored physical oceanographic data from northeastern Hudson Bay between August 1992 and September 1993. *Can. Data Rep. Hydrogr. Ocean Sci.* 132, 78.
- Saucier, F.J., Senneville, S., Prinsenberg, S., Roy, F., Smith, G., Gachon, P., Caya, D., Laprise, R., 2004. Modelling the sea ice-ocean seasonal cycle in Hudson Bay, Foxe Basin and Hudson Strait, Canada. *Clim. Dyn.* 23, 303–326.
- Serreze, M.C., Barrett, A.P., Slater, A.G., Woodgate, R.A., Aagaard, K., Lammers, R.B., Steele, M., Moritz, R., Meredith, M., Lee, C.M., 2006. The large-scale freshwater cycle of the Arctic. *J. Geophys. Res.* 111. doi:10.1029/2005JC003424.
- Shcherbina, A.Y., Gawarkiewicz, G.G., 2008. A coastal current in winter: autonomous underwater vehicle observations of the coastal current east of Cape Cod. *J. Geophys. Res.* 113, C07030. doi:10.1029/2007JC004306.
- Spall, M., Pickart, R.S., Fratantoni, P., Plueddemann, A., 2008. Western Arctic shelfbreak eddies: formation and transport. *J. Phys. Oceanogr.* 38, 1644–1668.
- St-Laurent, P., Straneo, F., Dumais, J.-F., Barber, D.G., 2011. What is the fate of the river waters of Hudson Bay. *J. Mar. Sys.* 88, 352–361.
- Straneo, F., Saucier, F., 2008a. The outflow from Hudson Strait and its contribution to Labrador Current. *Deep Sea Res.* 55, 926–946. doi:10.1016/j.dsr.2008.03.012.
- Straneo, F., Saucier, F., 2008b. In: Dickson, Meincke, Rhines (Eds.), *The arctic-sub arctic exchange through Hudson Strait, in Arctic-Subarctic ocean fluxes: defining the role of the Northern Seas in climate*, p. 740.
- Sutcliffe Jr., W.H., Loucks, R.H., Drinkwater, K.F., Coote, A.R., 1983. Nutrient flux onto the Labrador Shelf from Hudson Strait and its biological consequences. *Can. J. Fish. Aquat. Sci.* 40, 1692–1701.
- Sutherland, D.A., Pickart, R.S., 2008. The East Greenland coastal current: structure, variability, and forcing. *Prog. Oceanogr.* doi:10.1016/j.pocean.2007.09.006